Journal of Thermal Analysis and Calorimetry (2023) 148:9453–9464
https://doi.org/10.1007/s10973-023-12347-2

Preparation and thermal behavior of palmitic acid/activated carbon from corncob as phase change materials for thermal energy storage

Mohammad Alim Jafari[1,2] · Nursyafreena Attan[2] · M. Salim Tabish[4] · Anisa Amarkhil[2,3]

Received: 30 December 2022 / Accepted: 28 June 2023 / Published online: 14 July 2023

Abstract

In this research, the effects of activated carbon from corncob (ACC) biomass as the supporting material were investigated on leakage problem and thermal properties of palmitic acid (PA) as a phase change material (PCM) for thermal energy storage, using the impregnation method. The leakage test demonstrated that the addition of ACC significantly reduced the leakage of PA. Furthermore, it was evident from ATR-FTIR spectra and XRD results that PA and ACC did not undergo any chemical reactions, and the crystal structure of PA was not changed, while the ACC was amorphous. According to the SEM result, ACC had a porous structure, and its increase in PA caused a larger pore volume and a higher specific surface area, which could prevent the leakage of PA. The thermal stability of the composites was measured by TGA. The results revealed that the addition of ACC slightly accelerated the pyrolysis of PA, improved the thermal conductivity of PA, and had enough thermal stability below 150 °C to be suitable for building and solar thermal energy storage applications. DSC analysis of the form-stable PCM showed a melting temperature of 61.25 °C and a melting latent heat of 81.57 J g^{-1}, and demonstrated high thermal reliability after 10 cycles, indicating excellent energy storage capacity. The BET test revealed that the ACC with 1364.70 m2 g^{-1} have a great potential to use for supporting material, and the composites were mesoporous, which prevented the leakage of PA.

Keywords Thermal energy storage · Phase change materials · Fatty acid · Palmitic acid · Corncob · Activated carbon

Introduction

Energy consumption rises every year as a result of increasing global demand [1, 2]. Thermal energy storage (TES) based on phase change materials (PCMs) due to the small temperature difference and high enthalpy during the phase change process is one of the best energy storage methods to overcome the increase of energy consumption and balance the energy demand and its supply. PCMs can absorb and release huge amounts of thermal energy during the phase transition of freezing or heating with minimal volume changes [3, 4]. When the surrounding temperature reaches the PCM's melting point, it begins to store a certain amount of latent heat, which is later released in the same amount during its solidification process, and it is the energy storage mechanism of PCMs [5]. Appropriate phase change temperature, high latent heat, favorable phase change kinetics (melting/crystallizing quickly and repeatedly at a constant temperature or within a narrow temperature range), high thermal conductivity, enough thermal stability for the applications, free of leakage, cheapness, and nontoxicity are the important properties of PCMs [6, 7]. PCMs have a wide range of applications, including building energy conservation [8], thermal solar energy storage [9], temperature regulating textiles [10], refrigeration systems [11] food storage, and waste heat recovery. PCMs are classified as organic, inorganic, and eutectic PCMs [1]. Organic PCMs possess significant thermal stability, work in a large temperature range, non-toxicity [7], and resistant corrosion to making them a suitable source for PCMs [2, 7]. Fatty acids are a type of organic PCMs, that have little volume change during melting or solidification, and higher phase transition qualities than paraffin, although they are more expensive [12]. Palmitic acid is a widely accessible

✉ Mohammad Alim Jafari
alim.mozaffary1396@gmail.com

1 Daikundi Higher Education Institute, Nili, Daikundi 4201, Afghanistan

2 Universiti Teknologi Malaysia, 81310 Skudai, Johor Baharu, Johor, Malaysia

3 Kabul University, 3rd District, Kabul 1001, Afghanistan

4 Ghazni University, Qala Jowz, Ghazni 2301, Afghanistan

fatty acid with high thermal properties when implanted with supporting materials, and it is utilized as an eutectic phase change material with other PCMs too [13]. However, the low thermal conductivity, which reduces the heat transfer efficiency of thermal storage devices, and leakage problem during the phase transition of solid to liquid are the challenges of organic PCMs [7, 14–16]. Leakage can be solved through many methods, such as encapsulation [17], polymer matrix [18], and porous material adsorption [19]. Also, researchers have proposed several solutions to solve the low thermal conductivity, such as incorporation of metallic fins into the thermal storage system [20, 21], the mixture of multiple PCMs [22], the impregnation of highly conductive materials in the PCM [18, 23], encapsulation [24], and the fabrication of composite PCMs [25], but encapsulation and impregnation of the PCM in porous matrices are among the most commonly used methods [26]. Porous materials with a high porosity, large surface area, and high adsorption capacity have been widely used as supporting materials in the development of phase change material systems. During the phase transition change, the porous matrix can effectively prevent PCMs from leaking within the pores due to capillary action [27], and porous materials with excellent thermal conductivity and stability can further enhance the thermal conductivity of PCMs with varied temperature ranges too [28]. Moreover, supporting materials can decrease the flammability of organic PCMs [29]. Extensive research has focused on carbon-based materials as one of the best supporting materials for additives and encapsulation of PCMs due to their unique advantages, such as low density, superior thermal conductivity [30], intrinsic and structural flexibility, high chemical and thermal stability, and suitable characteristics [27]. Polyvinyl butyral (PVB) was used by Lin et al. [31] as a supporting material to prevent the leakage problem of PA, and expanded graphite (EG) was used to improve the thermal conductivity of PA, as well as decrease the leakage problem. Overall, scanning electron microscopy (SEM) images revealed a more distinct layer structure of PA with increasing PVB and EG content in the samples, which shows that supporting materials reduce the leakage of PA. Furthermore, the thermal conductivity of the FS-PCM is 0.5096 $W.m^{-1}$ K^{-1}, showing improvement and being higher than other samples without EG. The FSPCM, which contains 7:3 PA and PVB with a mass fraction of EG 7%, is a suitable candidate for application in low-temperature solar energy systems. Gu et al. [32] applied porous mullite and graphite powder to solve the leakage problem and improve the thermal stability of PA. When the mass fraction of mullite in PA/mullite/graphite is 70%, there is no leakage, as confirmed by experimental tests, and its thermal stability test shows that it is stable before 150 °C. Gu et al. [33] used carbonized pepper straw (CPS) as supporting materials to synthesize a novel FSPCM with the impregnation of PA. The resulting FSPCM (50% PA/50% carbonized pepper straw) has a latent heat of melting and solidifying of 95.5 J g^{-1} and 90.2 J g^{-1}, respectively. The FS-PCM also has no leakage and has the potential to be used for indoor heat systems.

In this present work, activated carbon from corncob (ACC) is used as a supporting material for the construction of a novel FSPCM due to its arrangeable porosity and high thermal conductivity, which were expected to solve the leakage problem and improve the thermal properties of PA. Using ACC as a supporting material, can reduce the accumulation of agricultural residues in the environment because corn to produce corncob waste is known as the 3rd largest agricultural crop in the world after wheat and rice [34], and according to some sources, for every 100 kg of corn grain produced, 18 kg of corncob is produced [35, 36]. It means there is a lot of corncob residue, which is usually discarded and burned to produce a lot of pollution in the air [34]. Biomass-derived porous carbon materials from renewable and cost-effective precursors are still in high demand among these porous carbon compounds [19]. Many scientists have been motivated to conduct research on activated carbon (AC) due to its numerous advantages [37]. Favourable AC possesses good chemical stability, arrangeable pore size and pore structure, and large surface area properties, which are commonly employed in catalysis, adsorption, and energy storage [38]. Besides that, during this process, corncob which is one of the most abundant agricultural wastes on the planet, is converted into a beneficial substance, that can help with the cleanliness of the environment [39]. Agricultural residues require an agent to activate them for the production of AC [40], which has effects on the porosity and volume of the pores of AC [41]. Several activating agents exist, such as sulphuric acid, potassium hydroxide [42], sodium hydroxide, phosphoric acid [38, 40] potassium carbonate, and zinc chloride. Phosphoric acid was used as a activation agent in this research because it is one of the non-polluting chemical agents that has been used more than others [41].

Material and experimental methods

Material

Corncob was collected from the vegetable market, Taman Universiti, and used as a precursor of AC. Phosphoric acid (purity is 99%), which is used as a chemical agent, and palmitic acid (purity > 98%), which is utilized as PCM were purchased from Merck KGaA (Germany) company.

Preparation of activated carbon from corncob

Agricultural waste corncob was collected from the Vegetable Market, Taman Universiti, Johor Bahru. Then, the

Table 1 Composition ratio of PA/ACC composites

Composites	PA/g	ACC/g	Ratio of PA and ACC	Mass percentage of PA/%	Mass percentage of ACC/%
PA/ACC-1	5	0.5	10:1	90.90	9.09
PA/ACC-2	5	1	10:2	83.33	16.66
PA/ACC-3	5	1.5	10:3	76.92	23.07
PA/ACC-4	5	3	10:6	62.5	37.5
PA/ACC-5	7	0.5	14:1	93.33	6.66
PA/ACC-6	7	1	14:2	87.5	12.5
PA/ACC-7	7	1.5	14:3	82.35	17.64

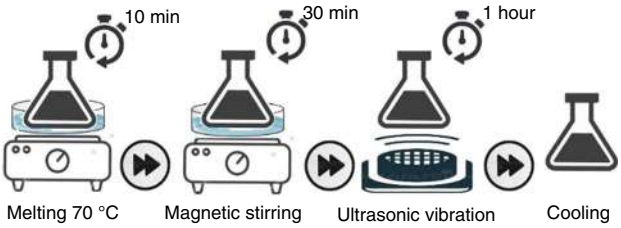

Fig. 1 Schematic diagram of PA/ACC composite preparation process

collected corncob was fragmented and washed by using tap water and distilled water several times. The washed corncob was then dried in the oven at 110 °C for 24 h. After that, approximately 50 g of dried corncob was placed in 500 mL of H_3PO_4 30% and soaked for 26 h at room temperature. Following this, the sample was dried in the oven overnight prior to calcination. The dried, impregnated corncob was placed into crucibles and calcined at 600 °C for 2 h in an electric furnace (Nabertherm B170 model).

Preparation of PA/ACC composites

PA and ACC were measured in separate beakers using an analytical balance according to Table 1. PA/ACC samples were prepared by melting a certain amount of PA on a hot plate through the water bath system at 70 °C for 10 min. A particular amount of ACC was then added to the respective amount of melted PA. To generate homogeneous mixture, each mixture was magnetically stirred for 30 min before being ultrasonically vibrated for 1 h. The corresponding schematic diagram of the preparation stages is shown in Fig. 1.

Leakage test

One essential criterion for evaluating PCMs' potential in future applications is their form stability. As a procedure, Han et al. [43] placed the composites on filter paper and then heated them in an oven to determine their leakage behavior. Each of the PA/ACC composites was subjected to a leakage test twice to see whether there was any leakage. The leakage tests of the PA/ACC composites were conducted using filter papers. On the filter paper, 1.0 g of each composite was placed and heated at 70 °C for 30 min in the oven. The mass of the composites before and after the test was recorded to measure the leakage percentage of the samples according to Eq. 1.

$$\%\ \text{leakage(mass loss)} = \frac{\Delta_{\text{mass}}\text{Paper}}{\text{mass sample}} \times 100 \quad (1)$$

Here, Δ_{mass}Paper was the mass difference of filter paper after and before the test, and mass samples were the initial mass of PA/ACC sample, which is adapted with the study of [44].

Characterization

ATR-FTIR (Parkin Elmer 100 Series) was used to determine the functional group of PA and PA/ACC composites. All samples were characterized in the 650–4000 cm^{-1} wavelength region, which corresponds to the ATR wavelength. The crystal structure and crystallinity of ACC and PA/ACC-4 as a sample of the highest concentration of ACC, and PA/ACC-5 as a sample of the lowest concentration of ACC were determined by X-ray diffraction (XRD, Rigaku Smartlab). The scanning 2Θ arranged from the starting angle of 10° to the ending angle of 90° with a scanning rate of 3° m^{-1}. The surface morphology of ACC and PA/ACC-4 and PA/ACC-5 was observed using a SEM (JSM-IT300LV, JEOL), and the samples were coated with platinum before the examination. Both thermal stability and mass loss percentage of PA and PA/ACC composites were measured by TGA (Shimdzu; 00539) with 50 °C initial temperature, 500 °C final temperature, and 10 °C min^{-1} heating under a pure nitrogen atmosphere. The thermal properties such as melting temperatures, melting latent heats, freezing temperatures, and freezing latent heats of PA and PA/ACC composites were investigated by DSC (TA instruments; DSC25) between (30–80) °C range temperature and 10 °C min^{-1} heating–cooling rate under pure nitrogen atmosphere. PA/ACC-4 as a shape-stable phase change material was melted and crystalized for 10 cycles under the same circumstances by DSC to measure the thermal reliability of the sample. The pore structure of ACC, PA/ACC-4 and PA/ACC-5 was measured using nitrogen absorption and desorption experiments by BET technique (NOVAtouch 4LX) at 77 K after the samples were dried at 100 °C for 5 h.

Result and discussion

Leakage test result

Figure 2 shows the leakage spot for each sample. The blue circles indicate the leakage of excess PA that ACC could not adsorb. ACC did not show any leakage during the test. Pure PA with 35.98% leakage showed the largest leakage spot among all samples. The leakage spots in PA/ACC composites became smaller as the amount of ACC in PA increased, which is consistent with the findings in reference [45]. During the phase transition change, the porous matrix may effectively prevent PCMs from leaking within the pores due to capillary action [27]. Table 2 shows PA/ACC-4 with the highest concentration of ACC and minimum leakage, had 1.87% leakage, making it suitable for use as a FSPCM. PA/ACC-5 with the lowest concentration of ACC in PA and maximum leakage among all PA/ACC composites.

ATR-FTIR analysis

The ATR-FTIR spectrum of PA and ACC are shown in Fig. 3. There were almost no absorption peaks observed in the spectra of ACC because all functional groups of the corncob were already broken, completely. The spectrum of pure PA is similar to its composites, has six major absorption peaks in the spectrum, and there is no new peak in the PCM composites. The peaks at 2914 cm^{-1} and 2848 cm^{-1} are caused by antisymmetric and symmetrical stretching vibrations of the $–CH_2$ group, respectively. A peak appears at 1697 cm^{-1} due to the stretching vibration of the C=O group. The Shear bending vibration of $–CH_2$ and $–CH_3$ groups has a peak at 1470 cm^{-1}. The –OH functional group's out of

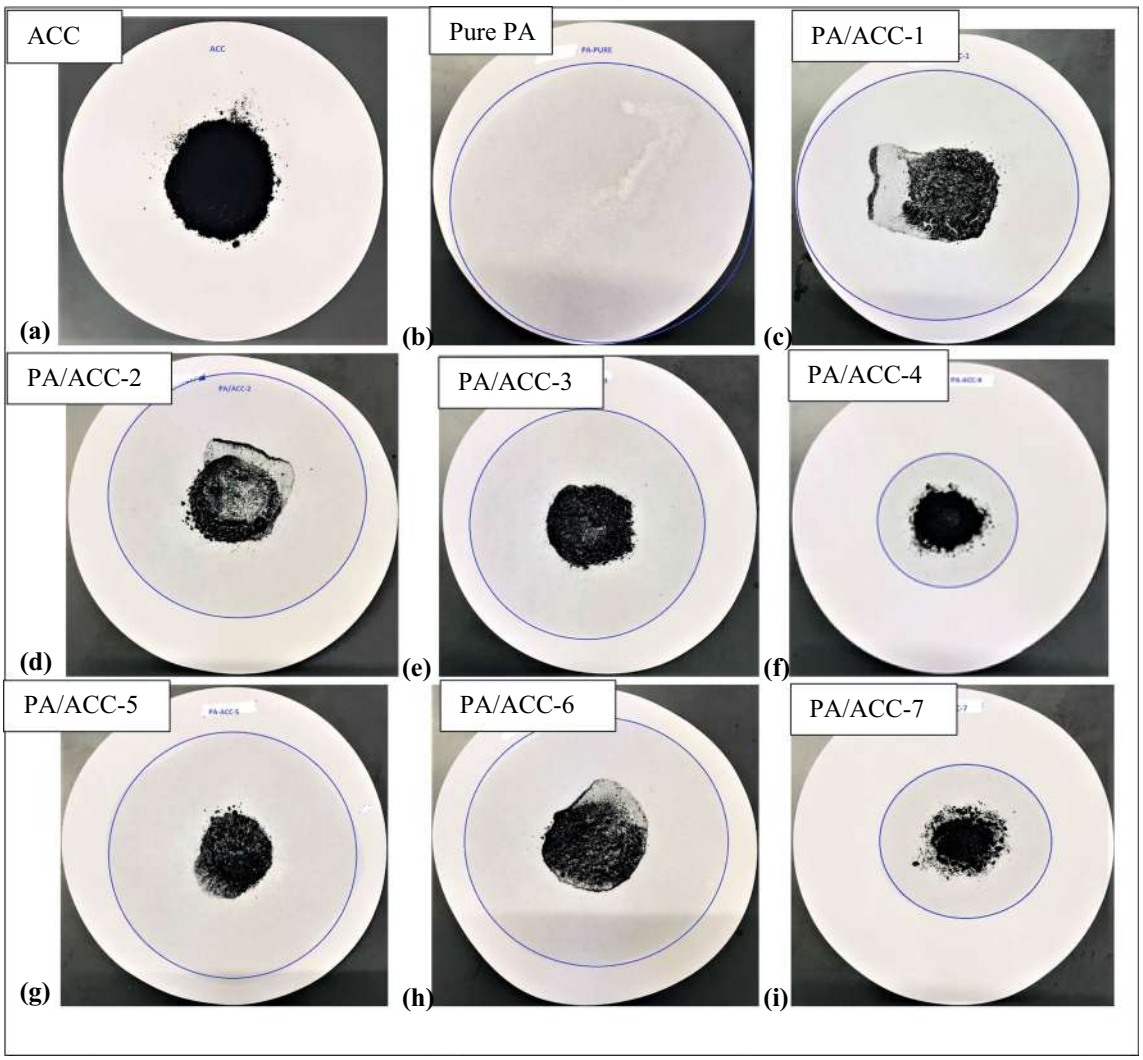

Fig. 2 Leakage tests of **a** ACC, **b** Pure PA, and **c**–**i** PA/ACC composites

Table 2 The leakage tests of PA, PA/ACC composites, and AC

Composites	PA/g	ACC/g	Initial mass/g	Final mass/g	Loss mass/g	Leakage/%
PA	1	–	1.0006	0.6405	0.3601	35.98
PA/ACC-1	5	0.5	1.0009	0.856	0.1449	14.47
PA/ACC-2	5	1	1.0003	0.9132	0.0871	8.70
PA/ACC-3	5	1.5	1.0009	0.9747	0.0262	2.59
PA/ACC-4	5	3	1.0018	0.983	0.0188	1.87
PA/ACC-5	7	0.5	1.0006	0.8289	0.1717	17.16
PA/ACC-6	7	1	1.0005	0.8684	0.1321	13.2
PA/ACC-7	7	1.5	1.0000	0.9579	0.0421	4.21
AC	–	1	1.0000	1.0000	–	–

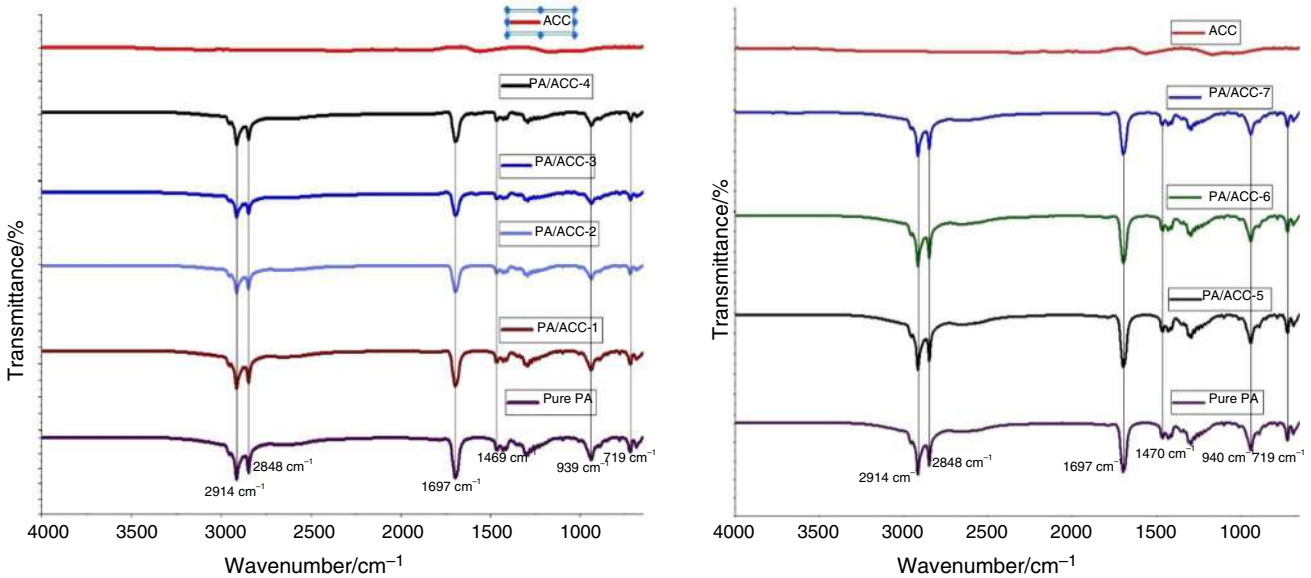

Fig. 3 The ATR-FTIR of PA, ACC and PA/ACC-1 to PA/ACC-7 composites

plane bending and in-plane swinging vibrations result in absorption maxima at 940 cm^{-1} and 719 cm^{-1} respectively, which corresponds with the findings of [31, 33]. As a result, PA and ACC are combined by surface tension and capillary force, and the mixing among them is physical; consequently, there is no chemical reaction between them. The PA/ACC composites exhibited excellent chemical stability.

XRD analysis

Wan et al. [46] finding shows the XRD spectra of PA indicate two sharp peaks at 22.3° and 24.2°, which correspond with the regular crystallization of PA. Figure 4 shows the XRD spectra of PA/ACC-4 as the highest concentration of AC and PA/ACC-5 as the lowest concentration of AC in the PA/ACC composites, which showed two sharp peaks at 22.3° and 24.2° as well, and the ACC spectra. As a consequence, the synthesized ACC has amorphous form and has three extremely small diffraction peaks at $2\theta = 21.9°$, 23°, and 43°. These peaks are attributed to the presence

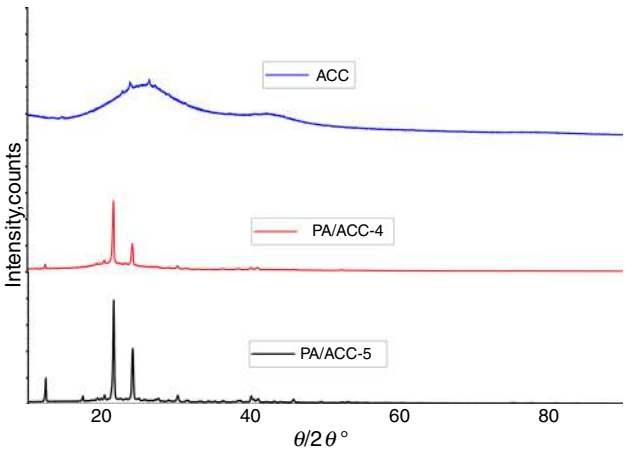

Fig. 4 XRD spectra of the PA/ACC-4 and PA/ACC-5 composites

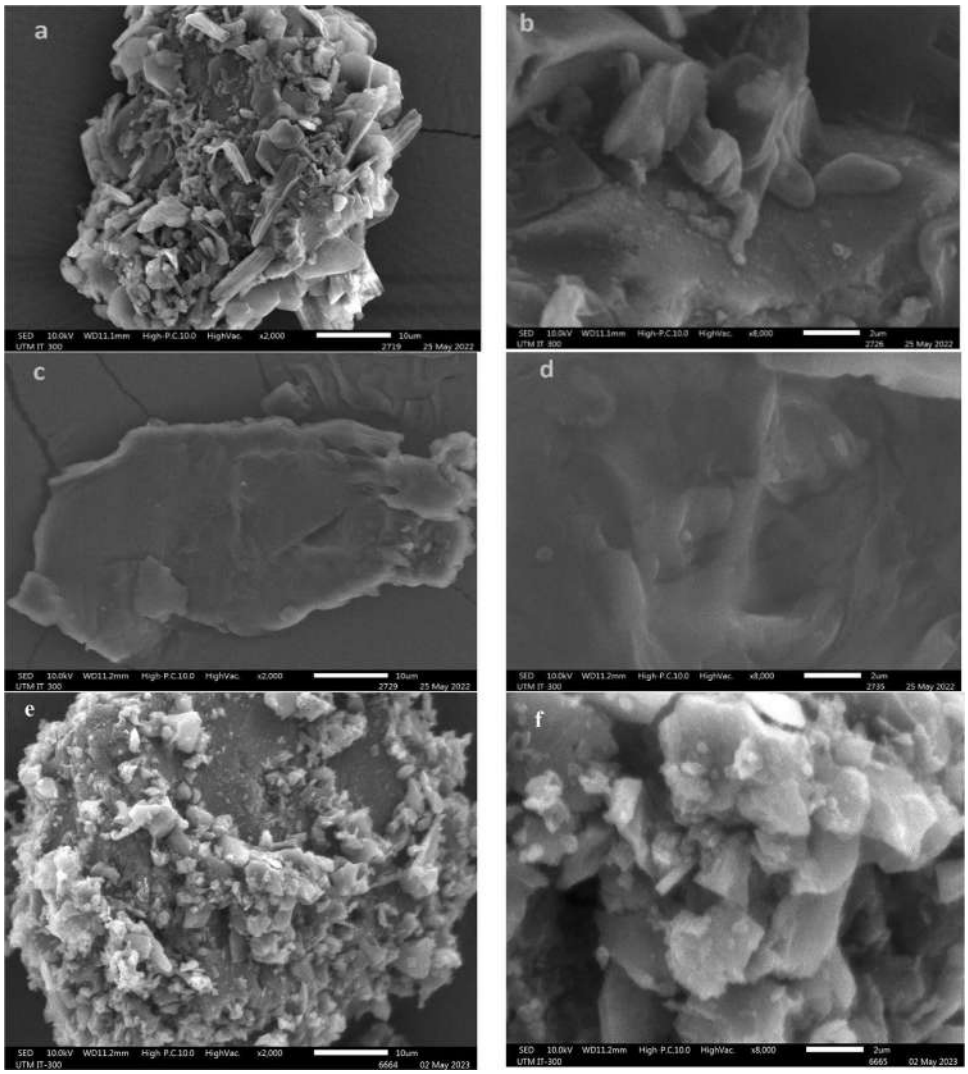

Fig. 5 The SEM morphology of PA/ACC-4 (**a**, **b**), PA/ACC-5 (**c**, **d**) and ACC (**e**, **f**)

of cristobalite in ash, which is consistent with the findings of [5, 47]. There was no chemical reaction between PA and ACC because the crystal structure of PA did not change. The peak of PA/ACC-4 spectrum was shorter than the PA/ACC-5 composite spectrum because of the higher mass ratio of ACC in it, which prevented the growth of PA crystal. PA/ACC-5 showed higher intensity than PA/ACC-4 due to the higher amount of PA in the composite.

SEM analysis

The SEM images in Fig. 5 show the cross-sectional images of PA/ACC-4, PA/ACC-5 composites, and ACC at lower (×2000) and higher (×8000) magnification. In Fig. 5a and b, the images of PA/ACC-4 with the highest concentration of ACC show rough and uneven fraction surfaces, while the images of PA/ACC-5 with the lowest concentration of ACC show smooth and flat fraction surfaces, as seen in Fig. 5c and d. The morphology of ACC in Fig. 5e, f features a well-developed porous structure, quite regular in shape, and multiple pores.

The size and shape of the surface structure became rough as the ACC concentration rose. This phenomenon is attributed to both the three-dimensional structure of ACC and the physical interaction between PA and ACC. The PA/ACC blended composites can keep their structure in the solid state during phase transition because of the interaction between PA and ACC, which is consistent with the finding of [48]. The outcomes showed that the ACC synthesized in this study had a porous structure that can adsorb PA, and the PA/ACC composites benefited from the large pore volume and high specific surface area of ACC by reducing the leakage of melted PA during the phase transition process, as adopted with the result [46].

TGA analysis

The TGA results of pure PA and PA/ACC composites were illustrated in Fig. 6. Each of the eight sets of samples has a single-step thermal decomposition process, and all of them obey the same mass loss principles. The pure PA and PA/ACC composites mass loss procedures are shown in Table 3. The mass loss of PA began at 166.45 °C and the mass loss ratio of the compound increased with the temperature rise and ended at approximately 275 °C. In comparison to pure PA, PA/ACC composites with additional ACC have earlier mass loss starting temperatures and quicker thermal decomposition rates. The addition of carbon particles enhances the PA/ACC composites' thermal conductivity and accelerated the pyrolysis of PA, which was adapted with the finding of [16]. The thermal stability of all PCM composites was significant for the application of buildings because the mass loss temperatures were largely higher than 50 °C, which is the maximum temperature used in construction buildings [49]. PA/ACC composites with favourable thermal stability below 150 °C were able to be used for solar thermal energy storage too. The degree of their thermal decomposition inhibition increases with the increase of carbon components percentage. Gao et al. [16] explained that the basic reasons for that are the secondary network structure created by ACC powder bridging and the overlapping porous network structure, which was caused by carbon material percentage increases and inhibits the thermal decomposition of PA in pores. As a result, PA/ACC-4 as FSPCM is the most suitable PCM compared to the other compositions for further applications.

DSC analysis

The phase change properties of the melting–freezing processes of pure PA, and PA/ACC composites are shown in Table 4 and Fig. 7, where the top curves represent the solidifying process, in which the heat is released, thus giving a heating effect, and the bottom curves represent the melting process, in which the heat is absorbed, thus giving a cooling effect. All PA/ACC composites curves and PA share a single peak value and the same curve change rule, it is evident from the figures that PA is fundamental to the latent heat in the phase transition process. The melting peak temperature and freezing peak temperature of pure PA are 61.56 °C and 59.32 °C, respectively. Compared with pure PA, the PA/ACC composites melting temperatures were lower as per the finding of [50], this difference is due to

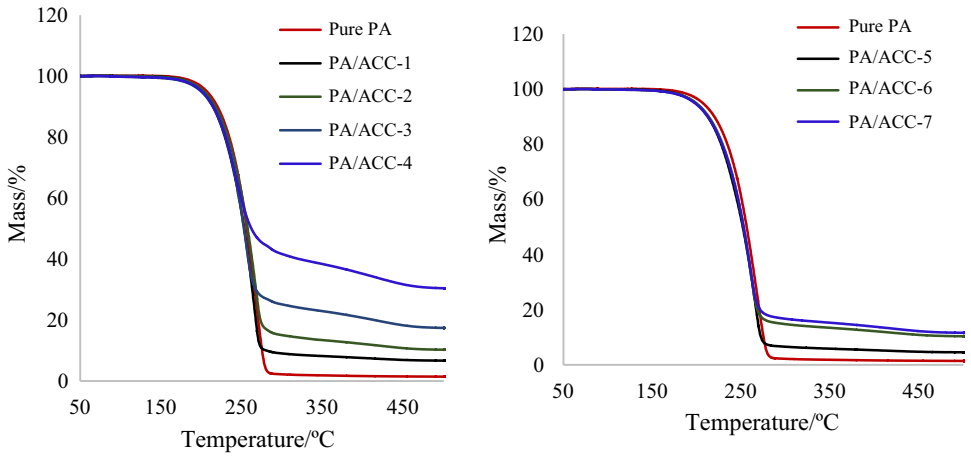

Fig. 6 TGA curves of PA and PA/ACC-1 to PA/ACC-7 composites

Table 3 TGA date of PA and PA/ACC composites

Composites	Initial decomposition temperature/°C	Maximal decomposition temperature/°C	Final decomposition temperature/°C	Mass loss/%
Pure PA	166.45	275	287.50	98
PA/ACC-1	160	271	302	90.25
PA/ACC-2	156	274	306	85
PA/ACC-3	150	267	300	75
PA/ACC-4	161.50	262	279	55.43
PA/ACC-5	156	270	296	93.50
PA/ACC-6	162	265	291	85.33
PA/ACC-7	157.70	265	295	83

weak interactions and a limited effect between PA and ACC. The melting latent heat range of PA/ACC composites was from 81.57 to 194.45 J g^{-1}, which is lower than the melting latent heat of pure PA (232.48 J g^{-1}). Also, the solidification latent heat range of PA/ACC composites was from 81.15 to 195.30 J g^{-1}, which was less than the freezing latent heat of 235.32 J g^{-1} for pure PA. The decrease in the latent heat of the PA/ACC composites may be attributed to the inhibitory effect of ACC on the crystallization of PA. It means ACC does not have latent heat; the latent heat of PA/ACC composites was reduced with the increase in carbon material mass fraction. When ACC was added since it prevented it from moving freely due to surface tension and capillary forces, which made it difficult for PA to crystallize. In addition, due to the smaller PA mass fraction, PA/CC-4 exhibited a lower enthalpy than other PA/ACC composites. Latent heat reduced as the mass fraction of ACC grew, indicating that the amount of heat energy required for the solid–liquid phase transition was decreased. Therefore, the freezing and melting temperatures decreased as well. The physiochemical characteristics may have changed as a result of ACC's dispersion.

Thermal reliability analysis

One of the crucial factors in determining whether PCM can be utilized for an extended period is thermal reliability. It was determined using the FSPCM thermal characteristics, which during leakage tests with 1, 5, and 10 heat cycles indicated the least leakage, as shown in Fig. 8 and Table 5. The melting and freezing points of the PA/ACC-4 after

Table 4 DSC data of PA and PA/ACC composites

Sample names	Melting		Freezing	
	Melting temperature/°C	Melting latent heat/J g^{-1}	Freezing temperature/°C	Freezing latent heat/J g^{-1}
Pure PA	61.56	232.48	59.32	235.32
PA/ACC-1	61.43	191.27	59.52	192.42
PA/ACC-2	61.37	163.91	59.49	162.71
PA/ACC-3	61.28	133.39	59.09	128.54
PA/ACC-4	61.25	81.57	59.62	81.15
PA/ACC-5	61.40	194.45	59.40	195.30
PA/ACC-6	61.39	173.10	59.64	170.77
PA/ACC-7	61.17	162.88	59.41	159.33

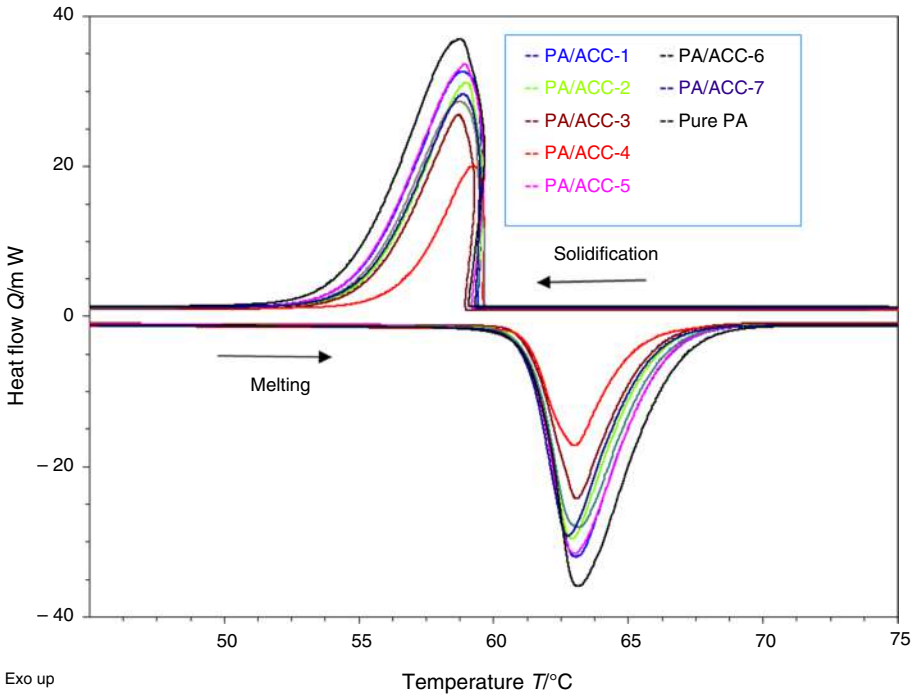

Fig. 7 DSC curve of PA and PA/ACC-1 to PA/ACC-7

10 cycles were only slightly different from their original points before the cycles, and the melting and freezing enthalpies changed little at all between the first and last 10 cycles. It means these changes had little effect on the characteristics of PA/ACC-4, as adapted to the findings of [51, 52]. It showed the sample of PA/ACC composites produced in this work and transformed into a FSPCM, had good thermal reliability as a consequence.

As a conclusion of thermal properties, the thermal properties of the FS-PCM in this research were compared to those of other FS-PCMs of PA with different supporting materials, as shown in Table 6.

BET analysis

In Fig. 9a and b, The PA/ACC-4 and PA/ACC-5 adsorption isotherm curves according to IUPAC classification were adapted to type (V) isotherms and H3 hysteresis loops, while the ACC curve adapted to type (IV) with H4 hysteresis loop. All samples were taking place in mesopores, capillary condensation with hysteresis which occurs between the desorption and the adsorption as explained in [53]. According to the IUPAC categorization based on pore size, mesoporous structures have pores between 2 and 50 nm [54]. As explained by McGlashan [55], the interactions between adsorbed molecules are stronger than the interactions between adsorbed and adsorbent. That is why the uptakes of gas molecules are slow at the beginning of interaction until the interaction between adsorbed and free molecules becomes stronger in this type of adsorption isotherm, as shown in Fig. 9a. As the concentration of ACC rises, the hysteresis loop becomes increasingly inclined, which is adopted with the finding of [56]. The capillary effects and surface tension forces were able to avoid the leakage of PA during phase change and when the temperature was above the melting point, according to the explanation in [57].

The BET-specific surface areas of ACC showed enough potential as a supporting material, and the porous volume of PA/ACC composites increased with increasing ACC, as shown in Table 7. The N_2 adsorption–desorption curve

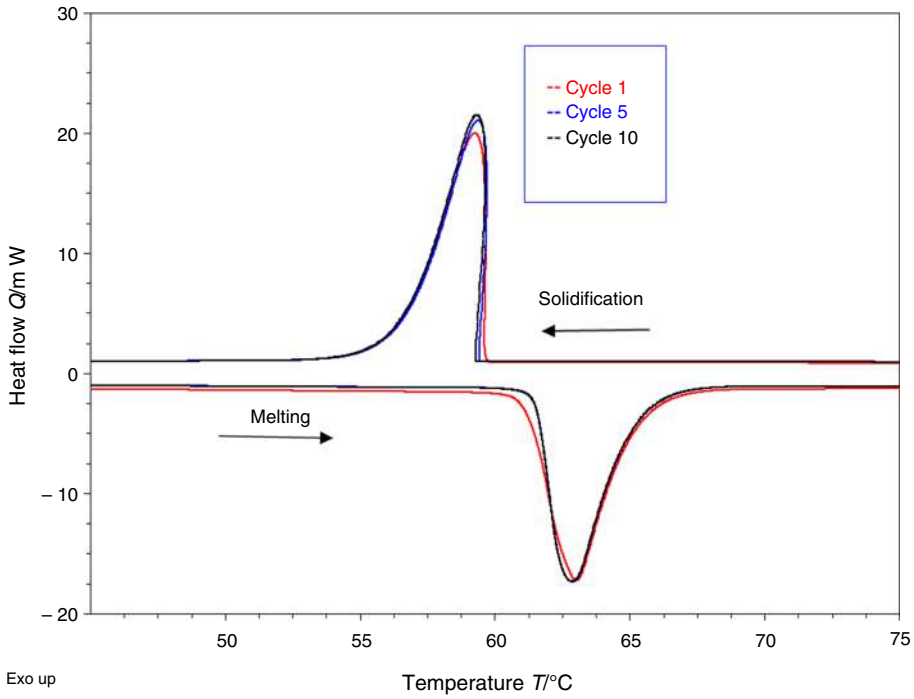

Fig. 8 DSC curves of PA/ACC-4 after thermal cycles

Table 5 DSC data of PA/ACC-4 (FSPMC) after thermal 10 cycle

Sample names	Melting		Freezing	
	Melting temperature/°C	Melting latent heat/J g^{-1}	Freezing temperature/°C	Freezing latent heat/J g^{-1}
Cycle 1	61.25	81.57	59.62	81.15
Cycle 5	61.43	80.00	59.57	80.495
Cycle 10	61.53	80.32	59.45	80.16

Table 6 Comparison of FS-PCM thermal properties of PA with different supporting materials

FS-PCM	Composition percentage/%	Latent heat		Decomposition Temperature			References
		Melting/J g^{-1}	Solidifying/J g^{-1}	Initial T/°C	Final T/°C	Mass loss/%	
PA/PVB/EG	65/28/7	122.05	121.99	245.90	483.30	13.10	[31]
PA/mullite/graphite	30/65/5	52.30	51.50	150	400	26.10	[32]
PA/mullite	32/68	50.80	58.30	200	600	28.19	[51]
PA/pinecone biochar	60/40	84.74	83.81	152	273	57.32	[46]
PA/ACC	62.50/37.50	81.57	81.15	161.50	279	55.43	This work

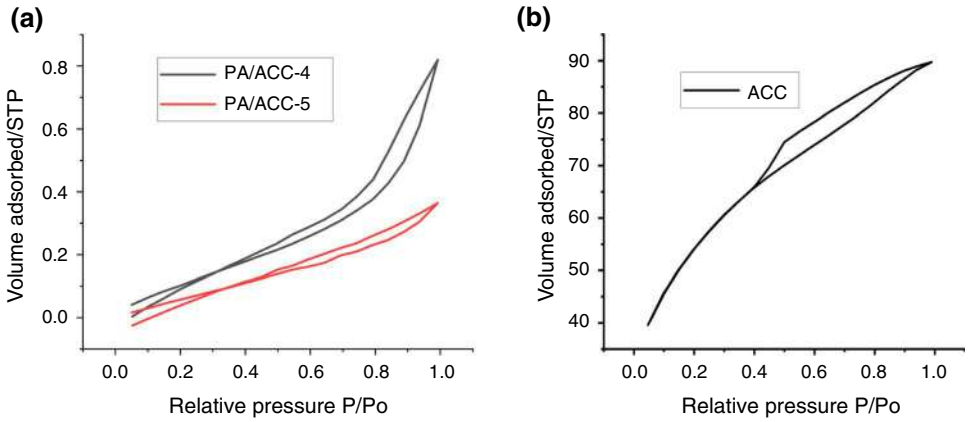

Fig. 9 The BET curves of PA/ACC-4, PA/ACC-5 (**a**) and ACC (**b**)

Table 7 Structural properties of PA/ACC composites

Sample name	Surface area/ m^2g^{-1}	Pore Vol/cm^3g^{-1}	Pore radius/nm
ACC	1364.70	0.3909	1.6812
PA/ACC-4	1.688	0.0039	1.5181
PA/ACC-5	1.344	0.0016	1.6900

showed that PA/ACC-4 has a higher surface area and a higher amount of adsorbed N_2 at all pressures than PA/ACC-5, as adapted with the finding of [58]. As a result, PA/ACC-4 can prevent the leakage problem of PA.

Conclusions

In this research, activated carbon from corncob was successfully synthesized and used as a supporting substance for palmitic acid to synthesize a novel FSPCM (PA/ACC-4). The results showed that the impregnation of ACC into PA improved the thermal properties, and prevented the leakage of melted PA during phase transition. The ATR-FTIR and XRD analyses confirmed that there was no chemical interaction between PA and ACC, and the SEM results demonstrated that synthesized ACC was a porous material that effectively adsorbed PA. The TGA results revealed that the FSPCM mass loss began at 161.50 °C and ended at 279 °C with 55.43% loss mass, which followed the same single step of PA thermal decomposition, which indicates that the thermal stability of the composite was desirable and suitable for building and solar thermal energy storage applications. As a consequence of the successful thermal properties of composites obtained by utilizing DSC, PA is the base of latent heat in the phase change transition process, and ACC doesn't have latent heat. The PA/ACC composites melting temperature, melting latent heat, and solidification were lower than PA because of the weak interaction between them and the existence of ACC, which caused a decrease in the crystallization value of PA. However, the melting point, solidifying point, melting latent heat, and solidifying latent heat of the FSPCM showed enough thermal storage capacity, which are 61.25 °C, 59.62 °C, 81.5 J g^{-1}, and 81.15 J g^{-1}, respectively. As well, the thermal characteristics of the FSPCM remained constant after ten cycles of the melting and freezing processes, which showed good thermal reliability and can be used in its applications. The BET results showed that ACC has a significant surface area (1364.70 m^2 g^{-1}) with the potential to be used as a support material. The composites with weak interaction between PA and ACC were mesoporous and possessed capillary

condensation, which could avoid the leakage of PA, and the specific surface area of them increased with the increase of ACC into PA. Overall, this study demonstrated that PA/ACC composites have promising potential for use in thermal energy storage applications.

References

1. Venkateswarlu K, Ramakrishna K. Recent advances in phase change materials for thermal energy storage-a review. J Braz Soc Mech Sci Eng. 2022;44:1–17.
2. Zhang Y, Zheng S, Zhu S, Ma J, Sun Z, Farid M. Evaluation of paraffin infiltrated in various porous silica matrices as shape-stabilized phase change materials for thermal energy storage. Energy Convers Manag. 2018;171:361–70.
3. Fu X, Liu Z, Wu B, Wang J, Lei J. Preparation and thermal properties of stearic acid/diatomite composites as form-stable phase change materials for thermal energy storage via direct impregnation method. J Therm Anal Calorim. 2016;123:1173–81.
4. Zhang Y, Zhang X, Xu X, Lu M. Derivation of thermal properties of phase change materials based on T-history method. J Energy Storage. 2020;27:1–10.
5. Göksu H, Aydınlı E, Hekimoğlu G, Sarı A. Activated carbon nanotube/polyacrylic acid/stearyl alcohol nanocomposites as thermal energy storage effective shape-stabilized phase change materials. Surf Interfaces J. 2022;31:1–10.
6. Tan N, Hao Y, Ping N, Yang H, Qi F, Chuan L, et al. Silica-confined composite form-stable phase change materials: a review. J Therm Anal Calorim. 2021;147:7077–97.
7. Yang H, Wang Y, Yu Q, Cao G, Sun X, Yang R, et al. Low-cost, three-dimension, high thermal conductivity, carbonized wood-based composite phase change materials for thermal energy storage. Energy. 2018;159:929–36.
8. Tofani K, Tiari S. Nano-enhanced phase change materials in latent heat thermal energy storage systems: a review. Energies. 2021;14:2–34.
9. Rolka P, Przybylinski T, Kwidzinski R, Lackowski M. The heat capacity of low-temperature phase change materials (PCM) applied in thermal energy storage systems. Renew Energy. 2021;172:541–50.
10. Yang K, Venkataraman M, Zhang X, Wiener J, Zhu G, Yao J, et al. Review: incorporation of organic PCMs into textiles. J Mater Sci. 2022;57:798–847.
11. Bukhalkin DD, Semenov AP, Novikov AA, Mendgaziev RI, Stoporev AS, Gushchin PA, et al. Phase change materials in energy: current state of research and potential applications. Chem Technol Fuels Oils. 2020;55:733–41.
12. Reddy KS, Mudgal V, Mallick TK. Review of latent heat thermal energy storage for improved material stability and effective load management. J Energy Storage. 2018;15:205–27.
13. Suresh Kumar KR, Kalaiselvam S. Experimental investigations on the thermophysical properties of CuO-palmitic acid phase change material for heating applications. J Therm Anal Calorim. 2017;129:1647–57.
14. Gao N, Tang T, Xiang H, Zhang W, Li Y, Yang C, et al. Preparition and structure-properties of crosslinking organic montmorillonite/polyurethane as solid-solid phase change materials for thermal energy storage. SSRN Electron J. 2022;244:1–10.
15. Rathore PKS, Shukla KS. Improvement in thermal properties of PCM/expanded vermiculite/expanded graphite shape stabilized composite PCM for building energy applications. Renew Energy. 2021;176:295–304.
16. Gao L, Sun X, Sun B, Che D, Li S, Liu Z. Preparation and thermal properties of palmitic acid/expanded graphite/carbon fiber composite phase change materials for thermal energy storage. J Therm Anal Calorim. 2020;141:25–35.
17. Qu Y, Wang S, Tian Y, Zhou D. Comprehensive evaluation of paraffin-HDPE shape stabilized PCM with hybrid carbon nano-additives. Appl Therm Eng. 2019;163:1–11.
18. Zhao X, Zou D, Wang S. Flexible phase change materials: preparation, properties and application. Chem Eng J. 2022;431:1–17.
19. Zou Z, Wu W, Shen W. Introduction of phase change material into sustainable carbon materials for enhanced shape stability and thermal conductivity. ChemistrySelect. 2020;5:8679–86.
20. Mahdi JM, Lohrasbi S, Nsofor EC. Hybrid heat transfer enhancement for latent-heat thermal energy storage systems: a review. Int J Heat Mass Transf. 2019;137:630–49.
21. Gao L, Fan X, Zhang S, Che D, Sun B. Palmitic acid graphene composite phase change materials: a molecular dynamics simulation. Thermochim Acta. 2022;707:1–8.
22. NL Narasimhan. Assessment of latent heat thermal storage systems operating with multiple phase change materials. J Energy Storage. 2019;23:442–55.
23. Jamil N, Kaur J, Pandey AK, Shahabuddin S, Hassani S, Saidur R, et al. A review on nano enhanced phase change materials: an enhancement in thermal properties and specific heat capacity. J Adv Res Fluid Mech Therm Sci. 2019;57:110–20.
24. Nagar S, Sharma K, Singh M, Kumar P, Pandey AK. Charging analysis and characterizations of COOH group functionalized graphene combined with paraffin wax as phase change material for thermal energy storage applications. J Therm Anal Calorim. 2022;147:11021–38.
25. Ahmadi O, Majidi S, Hashemi TP. Comparison of different approaches for thermal performance improvement of a phase change energy storage system. J Therm Anal Calorim. 2020;141:1753–68.
26. Cárdenas-Ramírez C, Gómez M, Jaramillo F. Characterization of a porous mineral as a promising support for shape-stabilized phase change materials. J Energy Storage. 2019;26:1–9.
27. Shi J, Qin M, Aftab W, Zou R. Flexible phase change materials for thermal energy storage. Energy Storage Mater. 2021;41:321–42.
28. Abdeali G, Bahramian AR, Abdollahi M. Review on nanostructure supporting material strategies in shape-stabilized phase change materials. J Energy Storage. 2020;29:1–31.
29. Muzhanje AT, Hassan MA, Ookawara S, Hassan H. An overview of the preparation and characteristics of phase change materials with nanomaterials. J Energy Storage. 2022;51:1–22.
30. Wu MQ, Wu S, Cai YF, Wang RZ, Li TX. Form-stable phase change composites: preparation, performance, and applications for thermal energy conversion, storage and management. Energy Storage Mater. 2021;42:380–417.
31. Lin Y, Zhu C, Alva G, Fang G. Palmitic acid/polyvinyl butyral/expanded graphite composites as form-stable phase change materials for solar thermal energy storage. Appl Energy. 2018;228:1801–9.
32. Gu X, Liu P, Bian L, He H. Enhanced thermal conductivity of palmitic acid/mullite phase change composite with graphite powder for thermal energy storage. Renew Energy. 2019;138:833–41.
33. Gu X, Liu P, Liu C, Peng L, He H. A novel form-stable phase change material of palmitic acid-carbonized pepper straw for thermal energy storage. Mater Lett. 2019;248:12–5.
34. Ibrahim SF, Asikin-mijan N, Ibrahim ML, Abdulkareem-alsultan G, Izham SM, Taufiq-Ya YH. Sulfonated functionalization of carbon derived corncob residue via hydrothermal synthesis route for esterification of palm fatty acid distillate. Energy Convers Manag. 2020;210:1–12.

35. Choi HJ. Agricultural bio-waste for adsorptive removal of crude oil in aqueous solution. J Mater Cycles Waste Manag. 2019;21:356–64.
36. Nazifa TH, Habba N, Salmiati, Aris A, Hadibarata T. Adsorption of procion red MX-5B and crystal violet dyes from aqueous solution onto corncob activated carbon. J Chin Chem Soc. 2017;65:1–12.
37. Rahma NA, Kurniasari A, Setyo Pambudi YD, Bintang HM, Zulfia A, Hudaya C. Characteristics of Corncob-Originated Activated Carbon Using Two Different Chemical Agent. In: 3rd MRS-ID meeting 2018. Depok, Indonesia IOP conference series: materials science and engineering. 2019. p. 1–7.
38. Xie XB, Wu D, Wu H, Hou C, Sun X, Zhang Y, et al. Dielectric parameters of activated carbon derived from rosewood and corncob. J Mater Sci Mater Electron. 2020;31:18077–84.
39. Zabi NZ, Ibrahim WNW, Hanapi NSM, Hadzir NM. Removal of various contaminants by highly porous activated carbon sorbent derived from agricultural waste produced in Malaysia—a review. Nat Environ Pollut Technol. 2021;20:1173–83.
40. Medhat A, El-Maghrabi HH, Abdelghany A, Abdel Menem NM, Raynaud P, Moustafa YM, et al. Efficiently activated carbons from corn cob for methylene blue adsorption. Appl Surf Sci Adv. 2021;3:1–8.
41. Amran F, Zaini MAA. Effects of chemical activating agents on physical properties of activated carbons—a commentary. Water Pract Technol. 2020;15:854–76.
42. Bakar NA, Othman N, Yunus ZM, Altowayti WAH, Al-Gheethi A, Asharuddin SM, et al. Nipah (*Musa acuminata balbisiana*) banana peel as a lignocellulosic precursor for activated carbon: characterization study after carbonization process with phosphoric acid impregnated activated carbon. Biomass Convers Biorefinery. 2021;5:1–8.
43. Han L, Ma G, Xie S, Sun J, Jia Y, Jing Y. Preparation and characterization of the shape-stabilized phase change material based on sebacic acid and mesoporous MCM-41. J Therm Anal Calorim. 2017;130:935–41.
44. Cárdenas-Ramírez C, Gómez MA, Jaramillo F. Comprehensive analysis of the thermal properties of capric-myristic, lauric-myristic and palmitic-stearic acids and their shape-stabilization in an inorganic support. J Energy Storage. 2021;34:1–10.
45. Sarı A, Bicer A, Al-Sulaiman FA, Karaipekli A, Tyagi VV. Diatomite/CNTs/PEG composite PCMs with shape-stabilized and improved thermal conductivity: preparation and thermal energy storage properties. Energy Build. 2018;164:166–75.
46. Wan Y, Chen Y, Cui Z, Ding H, Gao S, Han Z, et al. A promising form-stable phase change material prepared using cost effective pinecone biochar as the matrix of palmitic acid for thermal energy storage. Sci Rep. 2019;9:1–10.
47. Zhang Y, Song X, Zhang P, Gao H, Ou C, Kong X. Production of activated carbons from four wastes via one-step activation and their applications in Pb^{2+} adsorption: insight of ash content. Chemosphere. 2020;245:1–9.
48. Wu B, Fu W, Kong B, Hu K, Zhou C, Lei J. Preparation and characterization of stearic acid/polyurethane composites as dual phase change material for thermal energy storage. J Therm Anal Calorim. 2018;132:907–17.
49. Qu M, Guo C, Li L. Preparation, characterization and thermal properties of dodecanol, palmitic acid and hydroxylpropyl methyl cellulose as novel form-stable phase change materials. J Therm Anal Calorim. 2022;147:4915–24.
50. Wenbing J, Chaoming W, Zhengyu C, Wang T. Preparation and performances of palmitic acid_diatomite form-stable composite phase change materials. Int J Energy Res. 2021. https://doi.org/10.1002/er.5197.
51. Gu X, Liu P, Bian L, Peng L, Liu Y, He H. Mullite stabilized palmitic acid as phase change materials for thermal energy storage. Minerals. 2018;8:2–10.
52. Xing J, Zhou Y, Yang K, Chang J, Yu Y, Cai L, et al. Microencapsulation of fatty acid eutectic with polyvinyl chloride shell used for thermal energy storage. J Energy Storage. 2021;34:1–7.
53. Al-Ghouti MA, Da'ana DA. Guidelines for the use and interpretation of adsorption isotherm models: a review. J Hazard Mater. 2020;393:1–22.
54. McGlashan ML. Manual of symbols and terminology for physicochemical quantities and units. Pure Appl Chem. 1970;21:1–44.
55. Mg V, Rs D. A comprehensive investigation and artificial neural network modeling of shape stabilized composite phase change material for solar thermal energy storage. J Energy Storage. 2022;48:1–17.
56. Falahatian M. Preparation of paraffin/silica–graphene shape-stabilized composite phase change materials for thermal energy storage. J Mater Sci. 2022;33:12846–56.
57. Song X, Cai Y, Wang W, Sun X, Wu Y, Wei Q, et al. Thermal behavior and shape-stabilization of fatty acid eutectics/electrospun carbon nano-felts composite phase change materials enhanced by reduced graphene oxide. Sol Energy Mater Sol Cells. 2019;191:306–15.
58. Erdogan FO. Freundlich, langmuir, temkin, dr and harkins-jura isotherm studies on the adsorption of CO_2 on various porous adsorbents. Int J Chem React Eng. 2019;17:1–11.